Liquid Crystals
Publication details, including instructions for authors and subscription information:
http://www.informaworld.com/smpp/title~content=t713926090

The cholesteric-nematic transition in droplets subjected to electric fields

R. R. Swisher

Online publication date: 06 August 2010

To cite this Article Swisher, R. R.(1999) 'The cholesteric-nematic transition in droplets subjected to electric fields', Liquid Crystals, 26: 1, 57 — 62
To link to this Article: DOI: 10.1080/026782999205542
URL: http://dx.doi.org/10.1080/026782999205542

LIQUID CRYSTALS, 1999, VOL. 26, NO. 1, 57–62

The cholesteric–nematic transition in droplets subjected to electric fields

R. R. SWISHER, H. HUO, and P. P. CROOKER*

Department of Physics and Astronomy, University of Hawaii at Manoa,
2505 Correa Road, Honolulu, HI 96822

(*Received 31 June 1998; accepted 10 August 1998*)

We have observed the behaviour of chiral nematic droplets with positive dielectric anisotropy subjected to electric fields. With increasing field, the Frank–Pryce spherulitic director configuration is distorted progressively into a quasi-cylindrical spiral twist wall. As the field increases further this wall progressively unwinds, resulting in a *confined* cholesteric–nematic transition. Measurements of the pitch versus electric field show that, despite the confinement, the pitch is still described by the theory for the unconfined cholesteric–nematic transition.

1. Introduction

The study of liquid crystals in various confined geometries has recently been of great interest [1, 2]. Partly motivated by display applications, modes of confinement have long included boundaries formed by parallel plates, and more recently spherical surfaces (droplets) and invasive networks of polymerized threads. Interesting scientific questions also arise, however, resulting in studies of confinement in cylinders and, most recently, of internal confinement resulting from non-liquid crystalline droplets located within a larger liquid crystal droplet [3].

What configurations do confined liquid crystals take? For liquid crystals confined to spherical droplets, there are several possibilities [2]. For *nematics* with *perpendicular* boundary conditions, the texture may be *radial* (with a hedgehog point defect in the centre), or *axial* (with a ring defect lying on the equator). For nematics with *parallel* boundary conditions, the texture may be *bipolar* (with two surface defects at the poles) with a randomly oriented axis. The axis of such a bipolar drop can be oriented by an electric field—this is the basic mechanism of the polymer-dispersed liquid crystal display [4]. If, however, the droplet is *chiral nematic* (i.e. cholesteric), the texture is the Frank–Pryce texture [5], in which the twist axes are everywhere radial. For chiral nematics with *negative* dielectric anisotropy, application of an electric field changes the Frank–Pryce texture to a selectively reflecting configuration. Again, this transition is the basis for a reflecting display [6]. Similar textural changes have been demonstrated for chiral smectic (ferroelectric) liquid crystals [7].

*Author for correspondence.

Explanation of this behaviour always involves a competition between various aligning torques. For nematics without boundary conditions, torques on the director can only be balanced by parallel alignment. With spherical boundary conditions, however, an additional torque produced by the curved surface favours non-parallel alignment. By themselves, these two effects are sufficiently incompatible to cause topological defects—for example, a hedgehog within the droplet or polar surface defects.

If, in addition, an electric or magnetic field is applied, another competing torque is produced. Fields can modify the alignment or can relocate the defects and completely change the structure. In a chiral nematic, where torques in the unconfined material produce a natural twist, the situation is even more complicated. For such complex systems, textural instabilities may be caused by slowly varying an applied field [8], the boundary conditions [9], or the pitch [10]. Theoretical treatment of these systems is usually extremely difficult; as a result, any theory must usually be guided by experimental observations [11].

A related phenomenon, the cholesteric–nematic transition, occurs when external fields are applied to chiral nematics with positive dielectric anisotropy and pitch P_0. Here the torque produced by the field competes with the natural tendency of the chiral nematic to twist, causing a distortion of the twist and elongation of the pitch until, at some critical field E_c, the pitch becomes infinite and the liquid crystal becomes essentially nematic. For *unconfined* liquid crystals, this transition has been well described analytically [12]: $E_c = (K_{22}/\varepsilon_a)^{1/2}/P_0$, where K_{22} is the twist elastic constant and ε_a is the permittivity anisotropy. The question then arises as to how various confining geometries will

Journal of Liquid Crystals ISSN 0267-8292 print/ISSN 1366-5855 online
http://www.tandf.co.uk/JNLS/lct.htm
http://www.taylorandfrancis.com/JNLS/lct.htm

affect this transition. The situation for slab geometry with preset boundary conditions has been studied [13]; interestingly, confinement causes the unconfined second order transition to become first order. Similar questions are currently being investigated with respect to the way confinement affects *thermodynamic* phase transitions which are otherwise well understood in the bulk [14].

We present here the results of applying electric fields to chiral nematic droplets with *positive* dielectric anisotropy. Previous results by Kitzerow and Crooker [15] have shown that a spherically-confined, cholesteric–nematic transition does take place and that the critical field E_c is inversely proportional to the pitch as in the unconfined theory. Here we look at the process in more detail. At zero field, the texture is the well-known Frank–Pryce spherulite, which possesses radial twist axes and a radial $s = 2$ defect line. Application of the field results in a distortion and unwinding of the Frank–Pryce structure into an elliptically-, and then a cylindrically-spiral twist wall. As in the unconfined cholesteric–nematic transition, increasing field causes the overlapping sheets of this twist wall to become further separated, causing a progressive unwinding as the field increases. At the highest fields, this wall becomes a single, non-spiralling sheet. We show how this process takes place and we present measurements of the pitch versus applied field. Finally, we correlate our data with the theory for the unconfined cholesteric-nematic transition.

2. Experimental

Liquid crystals used in this experiment were a mixture of nematic ROTN-403 (Roche) doped with 0.687 wt % of the chiral additive S-811 (Merck). ROTN has dielectric anisotropy $\varepsilon_a = +19.2$; when mixed with S-811, the pitch of the mixture is 13.4 μm. This slightly chiral mixture was dispersed in a liquid matrix consisting of 75 wt % glycerol and 25 wt % polyvinyl pyrrolidone (Aldrich). The matrix provided the required parallel degenerate surface anchoring; the polyvinyl pyrrolidone provides sufficient viscosity to hold the droplets in place for the duration of a run without causing the spherical distortions which occur when drops are dispersed in solid or plastic matrices. Mixing was accomplished by first heating the two components of the matrix to 125°C; then, while at this temperature, several drops of the liquid crystal mixture were gently stirred in. Drops ranging in size from 15 to 200 μm were obtained; for this study, 80-150 μm drops were considered optimum.

Two sample cells were used in order to apply an electric field both parallel and perpendicular to the viewing direction. For electric fields parallel to the viewing direction (parallel observation), indium tin oxide-coated microscope slides separated by 250 μm glass spacers were used. For electric fields perpendicular to the viewing direction (perpendicular observation), two 170 μm thick copper strips were placed 250 μm apart between uncoated microscope slides and used as both spacers and electrodes. To minimize conductive effects, 1 kHz voltages were utilized across the respective conductors. The field was increased by $0.07\ \mathrm{V\,\mu m^{-1}\,h^{-1}}$ by amplitude-modulating the source signal with a computer-controlled ramp voltage. Observations were made with a Zeiss Universal microscope, both with and without crossed polarizers, using monochromatic sodium light ($\lambda = 589$ nm) in transmission. Images were observed with a video camera and recorded on a video tape recorder. Individual images could then be digitally captured and the pitch length, which corresponds to twice the ring spacing of a Frank–Pryce spherulite, measured using image-processing software.

3. Results and discussion

With no field applied (figure 1), the drops exhibit the classic Frank–Pryce spherulite texture [16]. (The videotape times on this and succeeding figures have no significance and can be ignored.) The circles are analogous to the chiral nematic fingerprint texture and are spaced by half the pitch length P. The line is

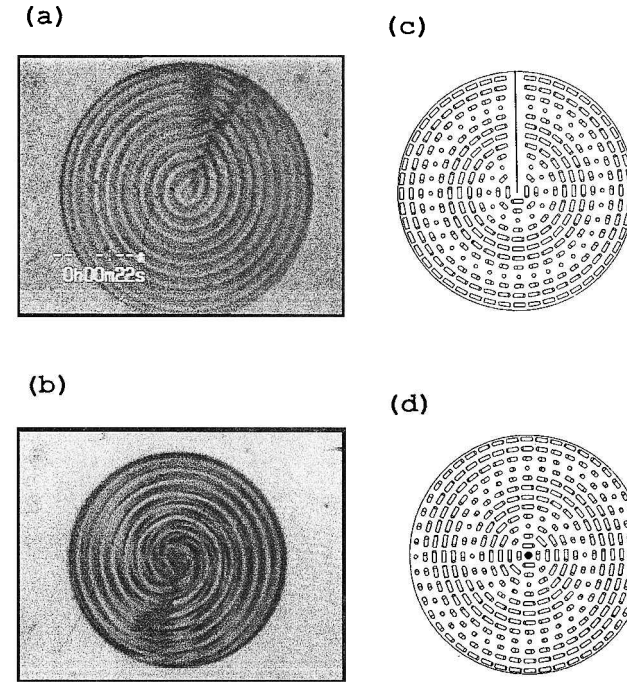

Figure 1. Droplet appearance for $E = 0$. (*a*) Droplet with defect approximately perpendicular to observation direction; (*b*) droplet with defect approximately parallel to observation direction; (*c*), (*d*) Frank–Pryce director configuration showing orientations for (*a*), (*b*), respectively. Only one pitch is shown in (*c*), (*d*) for clarity. (In this and succeeding figures, the numbers in the photos are videotape times and can be ignored.)

a χ disclination of strength 2 which can initially point in any direction. If the disclination lies in the plane perpendicular to the viewing direction, one observes circles with the defect lying along one radius [figure 1 (*a*)]. If, however, the disclination line is oriented along the viewing direction, the rings appear as a spiral and the disclination line itself is not visible [figure 1 (*b*)]. For both presentations, the distance between rings is in good agreement with measurements of the zero-field half-pitch in unconfined samples. The zero-field pitches for different droplets differed by $\pm 5\%$, however, since a new sample had to be made for each drop studied. To ensure that the measured pitch was not dependent on drop diameter, the zero-field pitch was measured for a range of droplets of diameters 20–150 μm both before and after electric field measurements. No systematic variation of the pitch with droplet diameter was observed.

Figures 1 (*c*) and 1 (*d*) show the zero-field Frank–Pryce director configurations corresponding to the photograph. The director is given by [16],

$$\mathbf{n} = \cos \Omega \mathbf{e}_\theta + \sin \Omega \mathbf{e}_\phi \qquad (1)$$

where

$$\Omega = \phi + qr. \qquad (2)$$

Here (r, θ, ϕ) are the usual spherical coordinates which give the director position, $q = 2\pi/P$ where P is the pitch, and the director lies in the plane perpendicular to the radius at angle Ω to the ϕ axis.

At zero field, the focus of the microscope is set so that the edge of the droplet is sharply defined. Application of a small field ($0.03\ \mathrm{V\,mm^{-1}}$) causes all drops to take on a spiral texture in parallel observation (figure 2), which indicates that the disclinations align with the field. However at fields above $0.1\ \mathrm{V\,mm^{-1}}$, the image becomes blurred with no movement of the drop itself, making measurement of the rings impossible. By changing the focus, the rings can be refocused, but it is still difficult to identify clear ring boundaries and a significant discontinuity is introduced in the graph of pitch versus field strength. Consequently we have not used pitch measurements obtained by parallel observation. Nevertheless, parallel observation provides a qualitative picture of the effect of the field: namely that at higher fields the lines tend to separate, which causes the spiral to unwind.

For perpendicular observation and small fields (figure 3), the defect is clearly seen to align with the field direction, consistent with parallel observation. Further increase in the field causes the rings to elongate into prolate ellipsoids and finally become lines parallel to the field. As the field increases, the lines become more widely separated, moving either toward the centre or toward the edge and disappearing at the higher fields. Since the focus setting remains the same for all fields, these images were used for pitch measurements.

Figure 4, which shows the director configuration in a more informative way, explains the behaviour. Figure 4 (*a*) depicts the director pattern in zero field. The

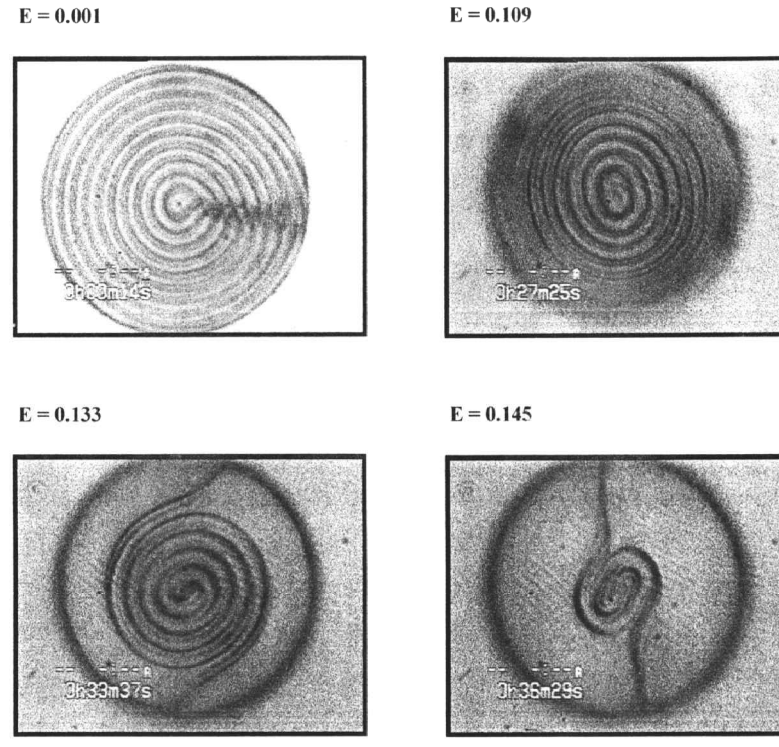

Figure 2. Parallel observations. As the field increases, the droplet changes focus (compare focus of droplet boundary) and the director field becomes a spiral twist wall. Note radial tendency of twist wall near the droplet periphery at high fields.

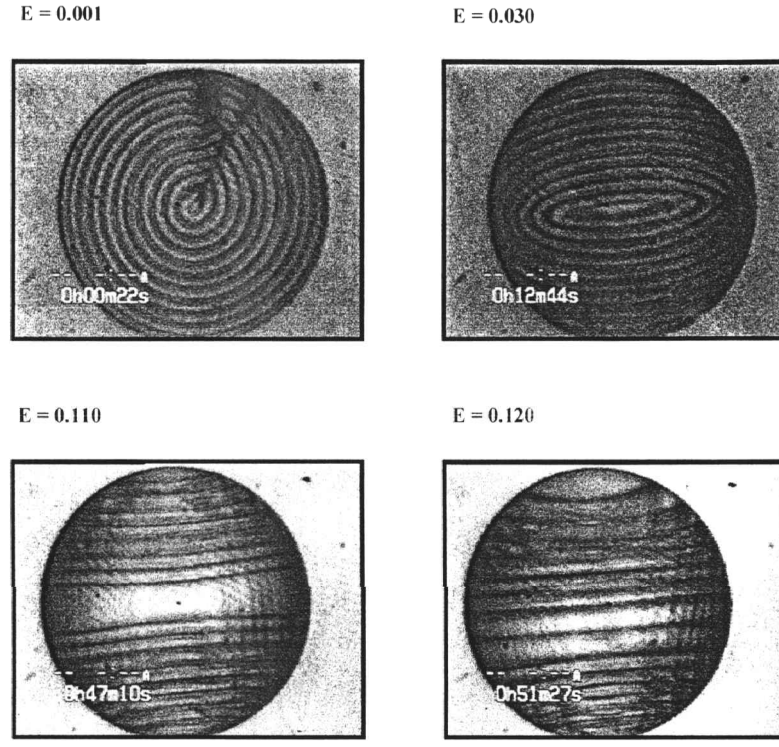

Figure 3. Perpendicular observations. The field is directed to the right; the defect aligns with the field and circles become elliptical and then straight lines. Lines tend to disappear through the centre or at the edge as the field increases.

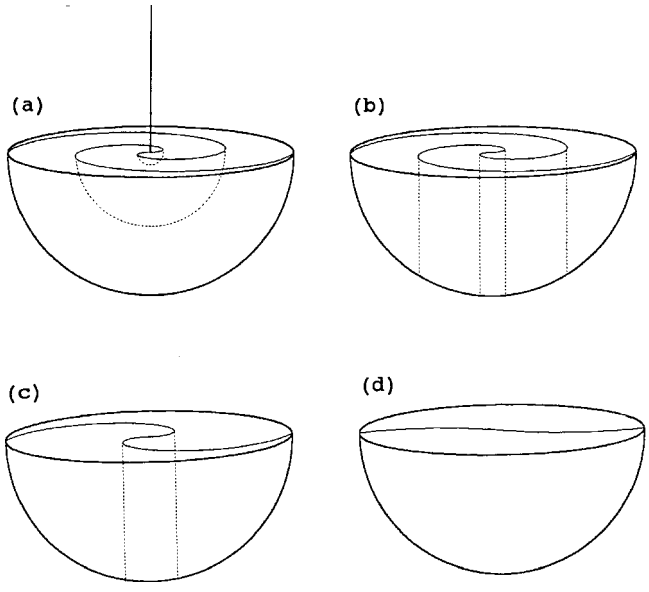

Figure 4. Evolution of droplet structure. The radial defect line is upward; surfaces represent the locus of points where the director is perpendicular to the radial defect. (*a*) Zero field case: a cross-section of the droplet shows a quasi-spherical spiral in the equatorial plane and circles in a meridional plane containing the defect. (*b*) Application of field E along the defect has caused the spiral to elongate into a quasi-ellipsoidal spiral, and finally into a cylindrically-spiral twist wall. (*c*) At higher fields, the twist wall becomes narrower and elongation of the pitch causes the spiral to unwind. (*d*) At high field, the spiral twist wall becomes a single planar wall; removal of this wall requires complete reorganization of the droplet.

defect line is upward; the spiralling sheet represents the locus of points on which the director is everywhere perpendicular to the defect line as previously depicted in figures 1 (*c*) and 1 (*d*). On the equatorial plane midway between the sheets, the director is parallel to the defect line; at all other points in the sphere the director is at some other angle to the defect line. The optical image verifies this model: notice that it appears as a spiral when viewed along the defect and as a circle when viewed perpendicular to the defect.

When an electric field is applied, the defect first aligns parallel to the field. At larger fields, alignment of those directors not parallel or perpendicular to the field causes the sheet to distort into an ellipsoidal spiral, and finally into a cylindrically-spiral sheet as shown in figure 4 (*b*). The sheet becomes a cylindrically-spiral twist wall with the directors off the sheet being essentially aligned with the field. The thickness of this sheet in the unconfined theory [12] is of order $\xi = (K_{22}/\varepsilon_a)^{1/2}/E$. Further increase of the field causes the thickness of the twist wall to decrease while increasing the distance between the spiral arms. The spiral therefore unwinds as shown in figure 4 (*c*) (see also figure 2). Eventually the spiral unwinds completely [figure 4 (*d*)], but expulsion of the final twist wall is frustrated by the spherical confinement and requires a discontinuous reorganization of the droplet [15].

We can now qualitatively explain why the parallel observations become blurred and out of focus when the field is applied. As the sheets elongate into ellipsoids, the

light transmitted through the droplet becomes channelled between the sheets for a relatively long distance, thereby creating a waveguide effect which distorts the image and refocuses the light. Since the length of each channel depends on the distance from the droplet centre, the new image is not in the same focus over the whole droplet. At high fields, where the sheets become cylindrically-spiral twist walls, the channels are as long as the droplet itself. The straightness of the channels improves the situation somewhat, but the presence of transverse refractive index gradients with different path lengths still causes focusing problems [17]. It is for this reason that measurements of the pitch length in parallel observation are untrustworthy.

The same model explains the perpendicular observations. The observed lines are the twist walls, shown as dashed lines in figure 4. As the pitch increases, the walls unwind, either from the centre or from the edge. If the edges are anchored, the twist walls disappear through the centre, but if the centre remains fixed, the walls disappear at the edge. We have observed both situations.

In practice, we observe that the outermost part of the sheet becomes *radial* (figure 2), rather than spiral as shown in figure 4. This effect is clearly a result of the spherical confinement, for which we at present have no explanation.

To provide a more quantitative description of the spherically-confined transition, measurements of the ring spacing versus electric field for droplets of diameter 86, 120, and 150 μm are shown in figure 5. Although it is tempting to associate the different critical fields E_c with the droplet diameter, it is necessary first to remove the effects of each droplet's slightly different zero-field pitch P_0. This has been done in the context of the theory for the unconfined transition [18], according to which there is a parameter a which goes from 0 to 1 as the electric field E goes from 0 to E_c. The field and pitch at any point are then given by

$$\frac{E}{E_c} = \frac{a}{E(a)} \tag{3}$$

and

$$\frac{P}{P_0} = \left(\frac{2}{\pi}\right)^2 E(a)K(a) \tag{4}$$

where $K(a)$ and $E(a)$ are complete elliptic integrals of the first and second kind, respectively. This theory suggests scaling the measured values of E and P for each droplet by the appropriate E_c and P_0. The results are shown in the inset to figure 5. Also plotted in the inset is the line corresponding to equations (3) and (4). Clearly the variation of pitch with field is well described by the unconfined theory.

It is interesting to speculate on the director configuration where the cylindrically spiral twist walls intersect the spherical boundary. One might expect that the incompatibility of a twist axis parallel to a surface with parallel degenerate boundary conditions would cause a distortion of the twist walls. From figure 2, however, their is no indication of the walls being affected by the surface. Either the electric field-aligned twist overrides the boundary conditions or any distortion is confined to a length much smaller than the pitch itself.

Finally, we have assumed that the parallel degenerate anchoring is strong—that is, the director at the surface is parallel to the surface itself or, equivalently, the surface extrapolation length for a non-parallel director is much smaller than the radius [19]. Extension of this study to very small radii would violate this condition and seem to be a good way to obtain information on the anchoring energy. Unfortunately, however, when the radius becomes comparable to the pitch, the patterns are much more difficult to interpret.

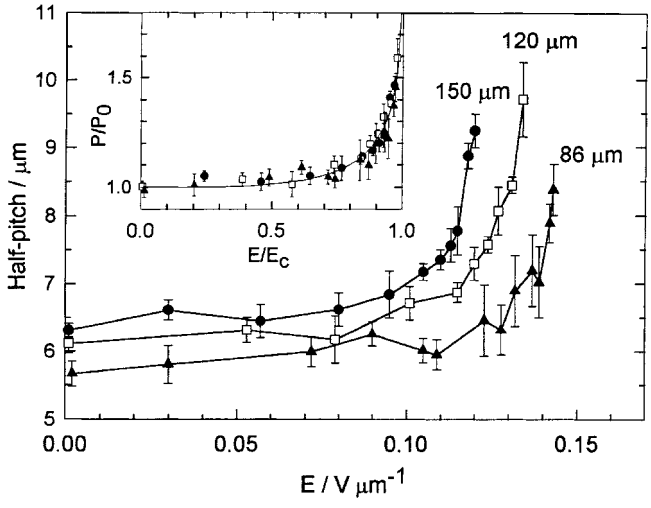

Figure 5. Half-pitch versus electric field for three droplet radii. Straight lines are guides to the eye. Inset: data scaled by the zero-field pitch and critical field; the line is from the theory for the unconfined cholesteric–nematic transition given in equations (3) and (4).

4. Conclusions

We have examined in detail the spherically-confined cholesteric–nematic transition and compared it with the same transition in an unconfined geometry. At low but non-zero fields, spherical confinement causes the twist walls to take the shape of a quasi-cylindrical spiral, with the spiral untwisting as the field increases and the pitch lengthens. From this model a defocusing effect which occurs in parallel observation is shown to be due to long channels with transverse refractive index gradients.

In addition, the model shows how the lines in the perpendicularly observed image disappear from the centre and edge of the sphere as the field increases. The increase of the pitch with field is well explained by the usual theory for the unconfined cholesteric–nematic transition. Finally, a tendency for the twist wall to become radial at the periphery of the droplet is still unexplained.

References

[1] Crawford, G. P., and Žumer, S. (editors), 1996, *Liquid Crystals in Complex Geometries* (London: Taylor and Francis) and references therein.

[2] Crooker, P. P., and Xu, F. D., 1998, in *Chiral Liquid Crystals*, edited by L. Komitov, S. T. Lagerwall, and B. Stebler (Singapore: World Scientific).

[3] Poulin, P., Stark, H., Lubensky, T. C., and Weitz, D. A., 1997, *Science*, **275**, 1770.

[4] Doane, J. W., Vaz, N., Wu, B.-G., and Žumer, S., 1986, *Appl. Phys. Lett.*, **48**, 269.

[5] Robinson, C., 1956, *Trans. Faraday Soc.*, **52**, 571; Robinson, C., Ward, J. C., and Beevers, R. B., 1958, *Discuss. Faraday Soc.*, **25**, 29.

[6] Crooker, P. P., and Yang, D. K., 1990, *Appl. Phys. Lett.*, **57**, 2529.

[7] Kitzerow, H.-S., Molsen, H., and Heppke, G., 1992, *Appl. Phys. Lett.*, **60**, 3093.

[8] Yang, D. K., and Crooker, P. P., 1991, *Liq. Cryst.*, **9**, 245; Xu, F., Kitzerow, H.-S., and Crooker, P. P., 1992, *Phys. Rev. A*, **46**, 6535; Xu, F., Kitzerow, H.-S., and Crooker, P. P., 1994, *Phys. Rev. E*, **49**, 3061.

[9] Volovik, G. E., and Lavrentovich, O. D., 1983, *Zh. eksp. teor. Fiz.*, **85**, 1997 (1983) (*Sov. Phys. JETP*, **58**, 1159).

[10] Xu, F., and Crooker, P. P., 1997, *Phys. Rev. E*, **56**, 6853.

[11] Lequeux, F., Hebd, C. R., 1986, *Acad. Sci. Paris II*, **303**, 765; Lequeux, F., and Kléman, M., 1988, *J. Phys. Fr.*, **49**, 845.

[12] De Gennes, P. G., 1968, *Solid State Commun.*, **6**, 163; Meyer, R. B., 1969, *Appl. Phys. Lett.*, **14**, 208.

[13] Durand, G., Leger, L., Rondelez, F., and Veyssie, M., 1969, *Phys. Rev. Lett.*, **22**, 227.

[14] Finotello, D., Iannachione, G. S., and Qian, S., 1996, in *Liquid Crystals in Complex Geometries*, edited by G. P. Crawford and S. Zumer (London: Taylor and Francis).

[15] Kitzerow, H.-S., and Crooker, P. P., 1993, *Liq. Cryst.*, **13**, 31.

[16] Bezi, J., and Žumer, S., 1992, *Liq. Cryst.*, **11**, 593.

[17] Saleh, B. E. A., and Teich, M. C., 1991, *Fundamentals of Photonics* (New York: Wiley), p. 18.

[18] Chandrasekhar, S., 1992, *Liquid Crystals*, 2nd Edn (New York: Cambridge University Press), p. 277.

[19] De Gennes, P. G., and Prost, J., 1993, *The Physics of Liquid Crystals*, 2nd Edn (Oxford: Clarendon Press).